International Journal Of
Industrial Electronics Control and Optimization
Print ISSN: 3517-2645
Online ISSN: 3568-2645
Homepage: https://ieco.usb.ac.ir/

Formation Control of Quadcopters with Unknown Target Tracking and Obstacle avoidance Using PID and MPC Controller

Seyedeh Mahsa Zakipour Bahambari | Saeed Khankalantary

Department of Electrical Engineering, K.N. Toosi University of Technology, Tehran, Iran..[1,2]
Corresponding author's email: s.kalantary@kntu.ac.ir

Article Info

Article type:
Research Article

Article history:
Received: 07-June-2024
Received in revised form: 07-November-2024
Accepted: 27-November-2024
Published online: 22-June-2025

Keywords:
Quadcopter,
Position Control,
PID Controller,
Tube-MPC,
Multi-Agent Systèmes Control

ABSTRACT

This article focuses on the design of a controller for quadcopter position control, which is then used to organize a group of quadcopters into a specific formation. Initially, PID controllers are developed to manage all output variables of the quadcopter systems efficiently. Subsequently, a constrained tube-model predictive control (Tube-MPC) approach is implemented to regulate the system's position, comparing its performance to that of the tube-MPC controller. The article also explores the coordination of a group of six quadcopters, focusing on achieving a predefined formation that maintains the desired shape. Three different scenarios are examined to control the formation, assessing how each approach influences the arrangement and coordination of the quadcopters. The dynamics of the system's control are crucial for effective operation in multi-agent systems. Moreover, the configuration of the quadcopters is influenced by each quadcopter's internal controller, ensuring accurate formation and tracking. This study underscores the significance of sophisticated control strategies in improving the performance and coordination of multiple quadcopter systems.

NOMENCLATURE

m	Quadcopter total mass	r_a	Obstacle radios
l	Length of quadcopter arm	K_r	Constant coefficient
I_x	Rotational inertial along the x-axis	K_a	Constant coefficient
I_y	Rotational inertial along y-axis	k	Constant coefficient
I_z	Rotational inertial along z-axis	q_o	Circle position
j_r	Rotor's inertial	λ_i	Constant coefficient
g	Acceleration due to gravity	t_s	Formation transition time
		τ	Exponential rate
		d_i^1	Desired distanc

I. Introduction

In recent years, the field of quadcopters, also known as quadrotor helicopters, has experienced a surge in interest. These UAVs and other unmanned aerial vehicles are no longer limited to military applications but have expanded into civilian, research, and commercial domains. Examples of application scenarios range from military and law enforcement surveillance and reconnaissance to fire monitoring, agricultural services, and nuclear reactor inspection.

The unmanned aerial vehicle (UAV) system is rapidly advancing and proving highly practical in unmanned systems. Its affordability, ease of use, and versatility make it a standout. Among UAV types, the quadrotor stands out for its ability to

Copyright © S. Khankalantary.
Publisher: University of Sistan and Baluchestan

hover, take off, land vertically, and fly indoors. As applications and mission requirements grow more diverse, single UAV capabilities are becoming constrained, highlighting the importance of coordinating multiple UAVs for formation flights in various scenarios [1-3]. A fleet of cost-effective UAVs has the potential to substitute costly multi-functional drones in extensive, high-precision missions, thereby boosting mission success rates[4]. The quadrotor's dynamics present a challenge due to having six degrees of freedom but only four inputs. This results in nonlinear, coupled, and under-actuated dynamics, making control difficult. Furthermore, during formation flight, quadrotors are susceptible to aerodynamic effects and random disturbances, necessitating advanced control strategies for stable, autonomous flight. Various strategies have emerged to address these control challenges in formation flight. For instance, Fu et al. delved into algorithms that maintained and reconstructed formations by employing artificial potential fields [5]. While the initial dynamic model of quadcopters is the starting point for all studies, subsequent research has introduced more complex aerodynamic features [6, 7]. Certainty-equivalent model predictive control (MPC) is a contemporary optimization-driven control method widely employed across diverse industrial processes[8, 9]. Wolfe et al. demonstrated the effectiveness of distributed multi-model Model Predictive Control (MPC) for tracking ground targets using quadrotors. The control algorithm was executed on the UAV's onboard computer[10]. Kuriki et al. developed a formation controller with obstacle avoidance capabilities by leveraging distributed Model Predictive Control (MPC) and a linearized model[11]. Additionally, from a geometric perspective, an NMPC design was introduced in [12] to address obstacle avoidance and enable aggressive trajectory tracking. Zhou et al. devised a controller for inward collision avoidance utilizing nonlinear Model Predictive Control (NMPC). Their approach involved a first-order model in two-dimensional space[13]. Unlike certainty-equivalent MPC, robust Model Predictive Control (MPC) offers a feasibility guarantee for the controlled system, typically within a specified uncertainty range[14]. In implementing MPC controllers, the computational time required to derive the feedback law is a major concern. Significant efforts have been dedicated to addressing certainty-equivalent MPC[15]. While the MPC framework has been introduced in previous studies[16, 17], there remains a necessity for additional reduction in computational burden within the control algorithms to facilitate the practical implementation of formation flight. The computational resources conserved could then be allocated to expanding the prediction horizon by employing a more precise UAV dynamics model. Model Predictive Control (MPC) has been utilized in quadcopter systems to track reference trajectories while accommodating disturbances. Additionally, nonlinear H-infinity techniques have enhanced the system's robustness[18]. Different control methods have been investigated for quadcopter control, including PID controllers[19, 20]. Moreover, in most articles related to quadcopters, the primary focus is on the impact of disturbances, addressing simulation results, and, to a large extent, not concentrating on experimental studies[21, 22]. In [23], the fundamental aspects of modeling and controlling quadcopters are discussed as a basis for further research and developments in this field. In the article mentioned above, the differential dynamic equations of a quadcopter are presented and simulated; then, stability is addressed by implementing a PD controller. Additionally, in [24], the motor model of a quadrotor is investigated using body equations and nonlinear simulation. Furthermore, algorithms and tracking models are being utilized to enable a quadcopter to track objects and perform optimal movements accurately[25]. In this study, after examining the mathematical model of a quadcopter and its motion equations, algorithms and controls related to object tracking are adjusted to track objects and perform optimal movements intelligently. In another study[26], a PID controller was designed to control a quadcopter's height, attitude, direction, and position. Subsequently, a PID controller is proposed for the nonlinear model, and the results are analyzed, concluding with a simple interfering PID controller for path tracking. Additionally, extensive research has been conducted on the group arrangement of quadcopters. For example, in[27], a distributed predictive model-based controller is suggested based on consensus theory for the group control of quadcopters. This controller addresses issues such as collision avoidance, obstacle avoidance, and maintaining communication topology during the movement of agents to achieve the desired formation. On a broader scale, a collision avoidance system based on herd decentralization by defining an anti-Laplacian matrix is provided[28]. Moreover, methods and regulations for arranging quadcopters are detailed and simulated in[29]. A robust model predictive control (MPC) approach has been proposed for quadcopter trajectory tracking, addressing the challenges of nonlinearity and disturbances by utilizing differential flatness for variable reformulation. This method transforms the trajectory tracking problem into the stabilization of a constrained linear time-invariant system, enabling effective control under disturbances. The approach is validated through simulations and experiments, demonstrating its capability to maintain robust tracking despite external disturbances in [30]. in [31] presents a tube-based nonlinear model predictive control (NMPC) strategy tailored for non-holonomic systems. The approach addresses the challenge of handling system constraints and disturbances by creating a robust control tube around the desired trajectory, ensuring stability and constraint satisfaction in real-time applications. In [32], formation control of quadcopters with mixed constraints is discussed, and other studies have investigated formation tracking control for a group of quadcopters with desired predefined trajectories in[33]. These challenges arise from

several factors, including the methodology used for control design, the need for effective communication among all agents, the potential for collisions, and the intrinsic complexity of quadcopter dynamics.[34, 35]. In [36], the author uses a leader-follower approach to form and control unmanned surface vehicle (USV) networks. The authors address the challenges posed by system uncertainties and stochastic disturbances in maintaining the formation. They propose a robust control method designed to handle these uncertainties and random disturbances, ensuring the stability of the formation. In [37] considered the DOCC of MASs with input saturation and collision avoidance constraints. On the other hand, [38] explore a method for localizing a radio frequency (RF) source by leveraging the presence of obstacles and their reflective properties. The authors propose a technique that uses a map of obstacles in the environment to enhance the accuracy of RF source localization. By accounting for reflections off surfaces, the method improves localization precision in complex environments where direct line-of-sight might be obstructed. The study demonstrates that incorporating information about obstacles and reflections significantly enhances the ability to pinpoint the RF source's location accurately.

The simulation results presented in the paper demonstrate the effectiveness of the proposed method under various environmental conditions and disturbances. The main contributions of this paper are as follows:

- Design a constrained Tube-MPC controller and compare it with a PID controller with a Disturbance
- Apply single-integrator formation to the nonlinear model with PID controller with three scenarios

This study begins by presenting the nonlinear and linear models of the quadcopter. Subsequently, a PID controller is crafted for the nonlinear model. The design process extends to developing PID and Tube-MPC controllers for the linear system. Furthermore, a continuous endeavor involves formulating a single integrator formation control for a fleet of six quadcopters, explicitly defining control inputs for tracking an unknown target. Lastly, the concluding section showcases simulations and outputs for each phase, facilitating a comprehensive comparative analysis.

The structure of this paper is outlined as follows: Section II describes the mathematical model of the quadcopter, while Section III presents the controllers. Section IV provides the formation control of a multi-agent quadcopter. Section V offers a simulation of controllers and formation of quadcopters. Lastly, the concluding remarks are shown in the final section.

II. Quadcopter Model

A typical quadcopter features four rotors arranged in a cross configuration. Adjusting the throttle involves simultaneously increasing or decreasing the speeds of all four rotors equally, generating a vertical force (U_1) in the body-fixed frame, which enables the quadcopter to ascend or descend. As shown in Fig. 1, controlling the roll movement involves increasing the speed of the left rotor while decreasing the speed of the right rotor. Similarly, pitch movement is controlled by applying the same process to the other two rotors. For yaw motion control, the quadcopter adjusts the front and rear rotors to rotate counterclockwise while the other two rotors rotate clockwise. This allows the quadcopter to perform a yawing maneuver by increasing the speed of the counterclockwise rotating motors and reducing the speed of the clockwise rotating motors.

Two reference frames are established to describe the dynamics of the quadcopter, as depicted in Fig. 1. The quadcopter's orientation is defined by three Euler angles: roll angle (θ), pitch angle (φ), and yaw angle (ψ). The vector $\Omega^T = (\varphi, \theta, \psi)$ represents these Euler angles, specifying the object's orientation. The vehicle's position in the inertial frame is given by the vector $r^T = (x, y, z)$The rotation matrix R is used to transform vectors from the body-fixed to the inertial frame. In this context, terms like $c\theta$ denote the cosine of θ, and $s\theta$ denote the sine of θ, facilitating the transformation between these frames.

$$R = \begin{bmatrix} c\psi.c\theta & c\psi.s\theta.s\varphi - s\psi.c\varphi & c\psi.s\theta.c\varphi + s\psi.s\varphi \\ s\Psi.c\theta & s\psi.s\theta.s\varphi + c\psi.c\varphi & s\psi.s\theta.c\varphi - c\psi.s\varphi \\ -s\theta & c\theta.s\varphi & c\theta.c\varphi \end{bmatrix} \quad (1)$$

Each rotor generates a thrust force perpendicular to its plane of rotation and produces an induction moment that opposes the rotor's direction of rotation. The thrust force for each rotor is specified as follows:

$$T = \sum_{i=1}^{4} |F_i| = b.\sum_{i=1}^{4} \omega_i^2 \quad i = 1,2,3,4 \quad (2)$$

where b represents the constant thrust coefficient, and w_i denotes the angular speed of each rotor [7]. The aerodynamic moment produced by the rotors is defined as follows:

$$\tau_i = d.\Omega_i{}^2 \quad i = 1,2,3,4 \quad (3)$$

where d is the constant drag coefficient of the propeller [7]. The external forces and torques acting on the quadcopter are determined according to criteria (3).

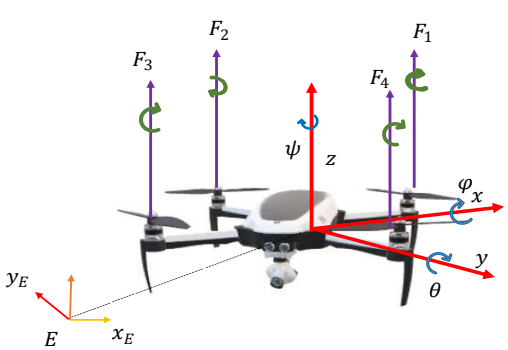


Fig. 1. Configuration inertia and body fixed frame

$$F_B = \begin{pmatrix} 0 \\ 0 \\ b(\omega_1^2 + \omega_2^2 + \omega_3^2 + \omega_4^2) \end{pmatrix} \quad (4)$$

The speeds produced are used to generate a relative speed, F_B, Which is required for quadcopter dynamics, as shown in Equation(4).

$$M = \begin{pmatrix} Lb(\omega_3^2 - \omega_4^2) \\ Lb(\omega_1^2 - \omega_2^2) \\ d(\omega_1^2 + \omega_2^2 - \omega_3^2 - \omega_4^2) \end{pmatrix} \quad (5)$$

the torque M consists of $\tau_\varphi, \tau_\theta, \tau_\psi$ which is the moment's input provided to the actuators to create the angular positional changes. L being the distance between the rotor and the center of mass of the quadcopter, d They can be explained in equation (5).

Overall dynamic model in the following form[38]:

$$\begin{aligned}
\ddot{x} &= -(\cos\varphi \cdot sin\,\theta \cdot \cos\psi + sin\varphi . sin\psi).\frac{U_1}{m} \\
\ddot{y} &= (\cos\varphi \cdot sin\,\theta \cdot cos\,\psi - sin\varphi . sin\,\psi).\frac{U_1}{m} \\
\ddot{z} &= -g + (\cos\varphi \cdot \cos\theta).\frac{U_1}{m} \\
\ddot{\varphi} &= \dot{\theta}\dot{\psi}\left(\frac{I_{yy} - I_{zz}}{I_{xx}}\right) - \frac{J_r}{I_{xx}}\dot{\theta}\Omega_r + \frac{\mathcal{L}}{I_{xx}}U_2 \\
\ddot{\theta} &= \dot{\phi}\dot{\psi}\left(\frac{I_{zz} - I_{xx}}{I_{yy}}\right) + \frac{J_r}{I_{yy}}\dot{\varphi}\Omega_r + \frac{\mathcal{L}}{I_{yy}}U_3 \\
\ddot{\psi} &= \dot{\theta}\dot{\varphi}\left(\frac{I_{xx} - I_{yy}}{I_{zz}}\right) + \frac{1}{I_{zz}}U_4 \\
\Omega_r &= (\omega_1 + \ \omega_2 + \ \omega_3 + \omega_4)
\end{aligned} \quad (6)$$

where g is the gravity coefficient, m is the mass of the quadcopter, φ, θ, ψ represent roll , pitch , and aw . I_{xx}, I_{yy}, I_{zz} is the total moment of inertia , J_r is the rotor moment of inertia, Ω_r is the total of gular speed , U_1, U_2, U_3, U_4 are th control inputs .

$$\begin{aligned}
\omega_1^2 &= \frac{T}{4K} - \frac{\tau_\theta}{2Kl} - \frac{\tau_\psi}{4b} \\
\omega_2^2 &= \frac{T}{4K} - \frac{\tau_\phi}{2Kl} + \frac{\tau_\psi}{4b} \\
\omega_3^2 &= \frac{T}{4K} - \frac{\tau_\theta}{2Kl} - \frac{\tau_\psi}{4b} \\
\omega_4^2 &= \frac{T}{4K} - \frac{\tau_\phi}{2Kl} + \frac{\tau_\psi}{4b}
\end{aligned} \quad (7)$$

$$U_1 = b(\omega_1^2 + \omega_2^2 + \omega_3^2 + \omega_4^2) \quad (8)$$

$$\begin{aligned}
U_2 &= b(\omega_3^2 - \omega_4^2) \\
U_3 &= b(\omega_1^2 - \omega_4^2) \\
U_4 &= d(\omega_1^2 + \omega_2^2 - \omega_3^2 - \omega_4^2)
\end{aligned}$$

Equation 7 is implemented to receive torques and generate the angular velocity of motors. Subsequently, the input control of the model dynamics is presented in Equation 6 .

$$\frac{d}{dt}\begin{bmatrix}\dot{\theta} \\ i_a\end{bmatrix} = \begin{bmatrix} -\frac{B_m}{J} & -\frac{K_t}{J} \\ -\frac{K_t}{J} & -\frac{R_t}{J}\end{bmatrix}\begin{bmatrix}\dot{\theta} \\ i_a\end{bmatrix} + \begin{bmatrix}0 \\ \frac{1}{L_a}\end{bmatrix}v \quad (9)$$

$$y = \begin{bmatrix}1 & 0\end{bmatrix}\begin{bmatrix}\dot{\theta} \\ i_a\end{bmatrix} \quad (10)$$

Equations 9 and 10 present the state-space model of the DC motor introduced in[39]The transfer function is derived and should be positioned within Block 3 before the equations by utilizing these equations. To linearize the above equations, ϕ ,and θ are considered small and ψ is considered to be zero. So that after linearization, they can be effectively neglected.

$$\begin{aligned}
\dot{X} &= AX + BU \\
Y &= CX + DU
\end{aligned} \quad (11)$$

$$A = \begin{bmatrix}
0 & 1 & 0 & 0 & 0 & 0 & 0 & 0 & 0 & 0 & 0 & 0 \\
0 & 0 & 0 & 0 & 0 & 0 & 0 & 0 & 0 & 0 & 0 & 0 \\
0 & 0 & 0 & 1 & 0 & 0 & 0 & 0 & 0 & 0 & 0 & 0 \\
0 & 0 & 0 & 0 & 0 & 0 & 0 & 0 & 0 & 0 & 0 & 0 \\
0 & 0 & 0 & 0 & 0 & 1 & 0 & 0 & 0 & 0 & 0 & 0 \\
0 & 0 & 0 & 0 & 0 & 0 & 0 & 0 & 0 & 0 & 0 & 0 \\
0 & 0 & 0 & 0 & 0 & 0 & 0 & 1 & 0 & 0 & 0 & 0 \\
0 & 0 & g & 0 & 0 & 0 & 0 & 0 & 0 & 0 & 0 & 0 \\
0 & 0 & 0 & 0 & 0 & 0 & 0 & 0 & 0 & 1 & 0 & 0 \\
-g & 0 & 0 & 0 & 0 & 0 & 0 & 0 & 0 & 0 & 0 & 0 \\
0 & 0 & 0 & 0 & 0 & 0 & 0 & 0 & 0 & 0 & 0 & 1 \\
0 & 0 & 0 & 0 & 0 & 0 & 0 & 0 & 0 & 0 & 0 & 0
\end{bmatrix} \quad (12)$$

$$B = \begin{bmatrix}
0 & 0 & 0 & 0 \\
0 & \frac{1}{I_x} & 0 & 0 \\
0 & 0 & 0 & 0 \\
0 & 0 & \frac{1}{I_y} & 0 \\
0 & 0 & 0 & 0 \\
0 & 0 & 0 & \frac{1}{I_z} \\
0 & 0 & 0 & 0 \\
0 & 0 & 0 & 0 \\
0 & 0 & 0 & 0 \\
0 & 0 & 0 & 0 \\
\frac{1}{m} & 0 & 0 & 0
\end{bmatrix} \quad (13)$$

$$C = I_{12\times12} \quad (14)$$

$$D = 0_{12\times4} \quad (15)$$

III. Control Scheme

In this section, the attitude control of the quadcopter is first investigated. Then, the position and attitude of the quadcopter are controlled. The PID, Tube-MPC algorithm is used for attitude and position control of the quadcopter.

A. PID Controller

At the beginning of this section, we design a PID controller for a non-linear system. In this context, we consider the reference values for both x and y to be 10 cm, and the reference value for z to be 20 cm. Moreover, the objective is to bring all angles to zero. The implementation diagram of the PID controller on the quadcopter is illustrated in Fig. 2 .

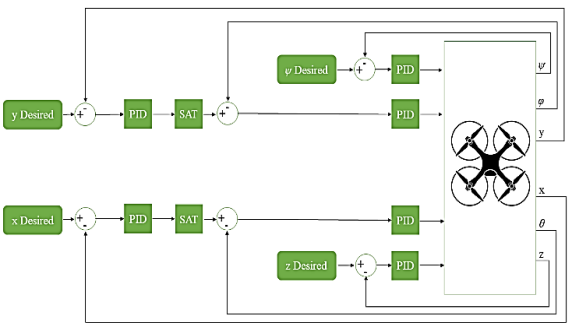


Fig 2. Control diagram for quadcopter system

In the design of the controller for the nonlinear system, the saturation value has been considered in the range of $-\frac{\pi}{36}$ to $\frac{\pi}{36}$. In this case, the PID controller coefficients are obtained through a trial-and-error method to achieve admissible settling time. The PID controller control equation is as follows:

$$u(t) = K_p e(t) + K_i \int e(t)dt + K_d \frac{de(t)}{dt} \qquad (16)$$

$$i = 1,2,3,4,5,6$$

In (16), K_p represents the proportional gain, K_i represents the integral gain and K_d represents the derivative gain. Furthermore, $e(t)$ represents the error between the desired value and the output.

In the Quadcopter system, there are six positional states (x, y, z) and three angular orientations (φ, θ, ψ). However, only four control inputs are available, represented by the angular velocities of the four rotors, denoted as ω_i. The relationship between these states and the total thrust (T) and torque (τ) generated by the rotors is described in the Quadcopter's dynamics, as shown in Equation (1) The total thrust (T) primarily affects the acceleration along the Z-axis, which is g the Z-axis, crucial for maintaining the Quadcopter airborne. Meanwhile, torque τ_φ influences the angular acceleration around the φ angle, torque τ_θ impacts the angular acceleration around the θ angle, and torque τ_ψ contributes to the angular acceleration around the ψ angle. As shown in Fig. 3.

$$\begin{aligned} T &= \big(g + u_1(t)\big) \times \frac{m}{cos\varphi . cos\theta} \\ \tau_\varphi &= \big(u_2(t)\big) \times I_{xx} \\ \tau_\theta &= \big(u_3(t)\big) \times I_{yy} \\ \tau_\psi &= \big(u_4(t)\big) \times I_{zz} \end{aligned} \qquad (17)$$

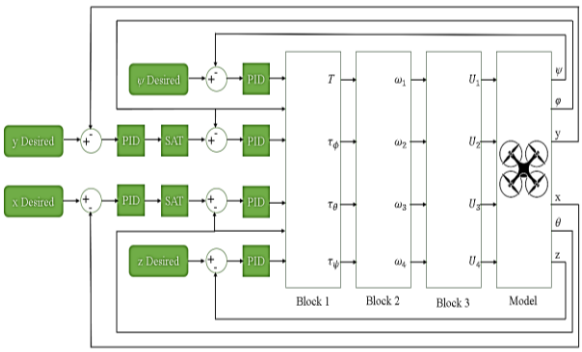


Fig. 3. Control nonlinear dynamic with motor dynamic schematic

B. Tube-MPC Control

This section addresses the design of a Tube-Model Predictive Control (Tube-MPC) for the position control of a quadcopter. Generally, the key advantages of this controller over a PID controller lie in its online nature and adaptability. However, it is worth noting that the Tube-MPC controller tends to be slower than PID, and its implementation on the system is consistently more challenging. The Tube-MPC Controller solves a finite-horizon optimal control problem with constraints on the system at each sampling instant. After solving the problem at each sampling time, it optimizes the system state and then computes the optimal solution for the new state in the next sampling time. To address Tube-MPC problems, the cost function is formulated as follows:

$$J_0(X(0), U_0) = p(X) + \sum_{k=0}^{N-1} q\big(X(K), U(K)\big) \qquad (18)$$

In which $p(x_N)$ represents a Lyapunov function in the form of $p(x_N) = X^T P X$, and $q(X(K), U(K))$ is a quadratic function expressed as $q(X(K), U(K)) = X^T Q X + U^T R U$. Additionally, U_0 denotes the input set over the time interval from 0 to $N-1$.

In general, the solution framework for Tube-MPC problems is as follows:

$$\begin{aligned} &J_0^*\big(X(0)\big) = \min_{U0} J_0(X(0), U_0) \\ &s.t.\ \ X_{k+1} = AX_k + BU_k \qquad k = 0, \dots., N-1 \\ &X_k \in \chi \ \ U_k \in \mathcal{U} \qquad k = 0, \dots., N-1 \\ &\left|\frac{dU}{dt}\right| \le constant \\ &X_N \in \chi_f \\ &X_0 = X(0) \end{aligned} \qquad (19)$$

N is the time horizon and χ, $\mathcal{U}$, χ_f are polyhedral regions.

The introduction of constraints results in a reduction of the adequate size of polyhedral regions. This reduction raises the possibility of encountering situations where a solution for the equation may not be feasible. In response, Tube-MPC controllers can be designed to offer maximum saturation, minimum saturation, or zero, aligning with the specific requirements of the target quadcopter.

The Tube-Model Predictive Control (Tube-MPC), functioning as an online controller, necessitates careful considerations when selecting a control or prediction horizon. Opting for a more extensive horizon may solve the system in a longer time step. Two strategies can be employed for those seeking solutions within a more minor time step. Firstly, one may reduce the control or prediction horizon, understanding that such an adjustment may impact system performance. Alternatively, the use of Explicit Tube-MPC offers a second solution. In this approach, the minimizing answer is computed and provided to the system as a function. However, this solution comes with the drawback of requiring substantial memory, rendering it both costly and resource-intensive. Consequently, quadcopters equipped with larger motors must effectively manage this added load.

Furthermore, in this article, all computations are done by Tube-MPC block in MATLAB-Simulink. Therefore, we designed a Tube-MPC controller by adding four PD controllers to the Tube-MPC block, for this Fig. 4 ., Present a block diagram in Simulink of MATLAB.

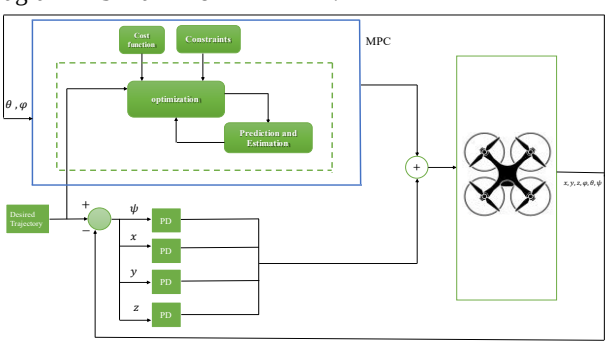


Fig. *4* . Tube MPC schematic

IV. Formation Controller

The proposed framework assumes that each quadrotor within the system senses the positions of other swarm members relative to a reference coordinate system. The control structure incorporates both inner and outer control loops. The inner loop is responsible for stabilizing the platform within a quadrotor, while the outer loop is dedicated to tracking a reference path. Due to the considerable difference in time constants between these two loops, they can be effectively decoupled into low- and high-level dynamics[40], Specifically, high-level dynamics are employed for swarm control, as shown in Fig. 5, which depicts a schematic representation of the controlled nonlinear dynamics in formation.

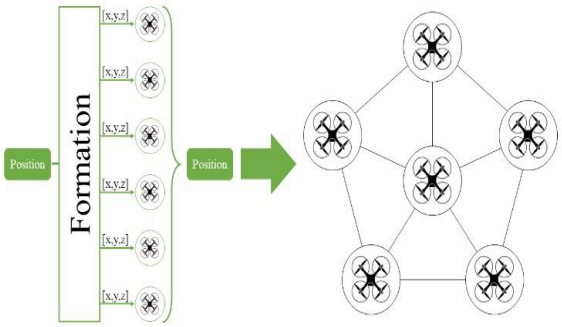


Fig. 5. Schematic Formalization of Nonlinear Controlled Systems

A. *Formation Helix*

This section aims to leverage the dynamics of a nonlinear quadcopter model to guide a subset of quadcopters toward a specific formation. To accomplish, this, we consider a group comprising six quadcopters .Ultimately, the goal is for all quadcopters to converge into a specific shape. The chosen formation strategy is based on a single-integrator integral-bilayer formation model. The noteworthy aspect involves integrating the dynamics of the nonlinear system controlled in Section Three into the formation strategy.

A nondirectional graph, denoted as G, can be defined as a tuple (V, E), where V represents the set of vertices (1, 2, …, n), and E is a subset of $V \times V$,Constituting the undirected edges. Notably, the inclusion of the vertex pair (i,j) in E implies the inclusion of its counterpart (j,i).

Given an arbitrary ordering of the edges in E, the edge function $\phi: \mathbb{R}^{nm} \rightarrow \mathbb{R}^{l}$ for a framework F = (G, q), where G = (V, E), is defined as follows [24]:

$$\phi(q) = \left[\dots, \left\|q_i - q_j\right\|^2, \dots\right], \quad (i,j) \in E \tag{20}$$

where q_i represents *i*'th agent position, and the kth component of (19), described as $\left\|q_i - q_j\right\|^2$Corresponds to the kth edge in E connecting vertices i and j. When delving into the infinitesimal rigidity analysis, a framework's rigidity matrix becomes a valuable tool. The rigidity matrix, denoted as $R: \mathbb{R}^{nm} \rightarrow \mathbb{R}^{l \times nm}$, is defined as:

$$R(q) = \frac{1}{2}\frac{\partial \phi(q)}{\partial q} \tag{21}$$

We also represent the relative position of the two agents as follows:

$$\tilde{q}_{ij} = q_i - q_j \tag{22}$$

And consider $\tilde{q} = [\dots, \tilde{q}_{ij}, \dots] \in \mathbb{R}^{ml}$ where $(i,j) \in E^*$, maintaining the same term order as defined in the edge function (19). The distance error is expressed as:

$$e_{ij} = \|\tilde{q}_{ij}\| - d_{ij} \quad (23)$$

Systems. If we consider $z_{ij} = \|\tilde{q}_{ij}\|^2 - d_{ij}^2$, According to (19), we can express the equation as follows:

$$z_{ij} = e_{ij}(e_{ij} + 2d_{ij}) \quad (24)$$

Given the above equations, we have the following theories:

Theorem1. Considering the formation $F(t) = (G^*, q(t))$, And assuming that the initial conditions of the error dynamics satisfy $e(0) \in \Omega_1 \cap \Omega_2$, where:

$$\Omega_1 = (e \in \mathbb{R}^l \mid \psi(F, F^*) \leq \delta),$$
$$\Omega_2 = (e \in \mathbb{R}^l \mid dist\big(q, Iso(F^*)\big)\ dist\big(q, Amb(F^*)\big)) \quad (25)$$

where δ represents a suitably small positive constant. The control law is defined as follows:

$$u = u_a := -K_v R^T(\tilde{q}) z \quad (26)$$

And $K_v > 0$ denoting a user-defined control gain. The introduced control law helps the system reach a specific form by considering the distance of agents from their desired values[29].

Theorem2. Considering the formation $F(t) = (G^*, q(t))$ with initial conditions on $e(0)$ as specified in Theorem 1, the control $u = u_a + 1_n \otimes h$, where $u_a = [u_{a1}, \dots, u_{an}]$ defined in (18), and $h = (K_1 + 1)e_T + \hat{v}_T - u_{an}$ Enables the agents to track an unknown object. Where $\hat{v}_T$ Represent target velocity that assumed to be measured by sensors and received by agent 6 and e_T defined.The proof of Theorem 1 and Theorem 2 has been presented in[29]

$$e_T = \begin{bmatrix} x_r \\ y_r \\ z_r \end{bmatrix} - \begin{bmatrix} x_{Agent\ 6} \\ y_{Agent\ 6} \\ z_{Agent\ 6} \end{bmatrix} \quad (27)$$

Formation and Obstacle Avoidance

The following section considers formation and obstacle avoidance in placing quads in a line formation while avoiding the sphere obstacle. The general equations of double integrator with obstacle avoidance can be written as follows:

$$\ddot{q}_i = u_i \quad (28)$$
$$u_1 = \ddot{q}_d + (\dot{q}_d - \dot{q}_1) + (q_d - q_1) + u_{oi} \quad (29)$$
$$r_i = \|q_i - q_0\| - R \quad (30)$$
$$u_i = \sum_j \frac{K_r(q_i - q_j)}{\|q_i - q_0\|} + \sum_j K_a\Big((q_j - q_i) + (\dot{q}_j - \dot{q}_i)\Big) \quad (31)$$

In the above equations, position is defined as $q = \begin{bmatrix} x \\ y \\ z \end{bmatrix}$. In this formation, even the leader gets control input, as shown in (29). The first part consists of the difference between desired acceleration, velocity, and position and the first agent's acceleration, velocity, and position. The second part of the control input (u_{oi}) Is added to avoid collision as follows:

$$u_{oi} = \begin{pmatrix} K\frac{q_i - q_0}{r_i^2}\left(\frac{1}{r_i} - \frac{1}{r_a}\right) & , r_i \leq r_a \\ 0 & , otherwise \end{pmatrix} \quad (32)$$

In (30), R is the radius of an obstacle, q_i is the position of ith agent and q_o is the position of obstacle (30) is the input control for other agents.

Variation formation

Variation formation in quadcopters, often termed formation control, involves the coordination of multiple quadcopters to maintain a specific spatial configuration during flight. This is achieved through leader-follower models, Model Predictive Control (MPC) The leader-follower approach ensures followers adjust their positions relative to a designated leader, maintaining formation integrity[41] MPC optimizes trajectories for obstacle avoidance and efficient movement, while MPC ensures robust convergence to desired formations despite disturbances. These advanced strategies are pivotal in applications such as surveillance, search and rescue, and environmental monitoring, allowing for precise and reliable multi-agent coordination.

In this section, system is same as the system in (22), even though formation changes after t_s and the relation and distance between agents is determined through the following equation

$$d_i = (d_i^1 - d_i^2)\big(1 - e^{-\tau(t - t_s)}\big)u(t - t_s) \quad (33)$$

According to (33), j and i in d_i^j show the position of the quad in varying formation and the ith agent, respectively. Then, control input is applied to system as follows:

$$u_i = \lambda_1(q_1 - q_i - d_i) + \lambda_2(\dot{q}_1 - \dot{q}_i) \quad (34)$$

V. Simulation and Results

This section explores three scenarios involving various modes of PID and Tube-MPC controllers and their behavior in the presence and absence of disturbances. Subsequent analysis illustrates Tube-MPC controllers' performance under disturbed and undisturbed conditions. Table 1 provides the constant values utilized in the quadcopter simulation.

It is important to note that this discussion is divided into two sections. In the first section, two internal controllers are designed and compared. The second section considers three scenarios for formation control using the selected controller.Table I. Model design parameter.

Table I. Model design parameter

Symbol	Parameter	Value	Unit
m	*Quadcopter total mass*	0.8	kg
l	*Length of Quadcopter arm*	0.3	*m*
I_x	*Rotational inertia along x − axis*	0.01567	kg.m^2
I_y	*Rotational inertia along y-axis*	0.01567	kg.m^2
I_z	*Rotational inertia along z − axis*	0.0283	kg.m^2
J_r	*Rotor's inertia*	6.01e-5	kg.m^2
g	*Acceleration due to gravity*	9.81	$m.s^2$

A. Comparison PID and Tube-MPC Controller

The mathematical model of the quadcopter vehicle and its associated control systems were constructed in MATLAB/Simulink to facilitate simulation. The primary goal of this analysis is to assess the control algorithms' efficacy in preserving the quadcopter's stability. The initial state assumes the quadcopter is in hover mode with specific pitch, roll, and yaw angles. Then, the quadcopter is commanded to transition into a stable state where these angles gradually approach their desired values. Both control strategies are applied in this scenario, and their outcomes are subsequently compared. The gains for the classical PID controller were determined using the Ziegler-Nichols method. We used this approach to determine the PID and Tube-MPC gain parameters presented in Table II. and Table III.

Furthermore, linearized equations are utilized to design the Tube-MPC controller on this system, with a sampling time of 0.001 considered. Moreover, a prediction horizon of 20 and a control horizon of 15 are chosen. On the other hand, the input and output weight values are denoted by $R = diag(0.73891,0.73891,0.73891,0.73891)$ and $Q = diag(10,1,10,0,1,1,100,10,100,10,100,0) \times 7.3891$, Respectively. It should be emphasized that all these values have been determined through trial and error. The coefficients of these four controllers are as follows according to Table III.

Table II. PID controller coefficients for the nonlinear system

	K_p	K_i	K_d
ψ	2	10	2
ϕ	3	10	2
θ	1	0	0.2
x	0.1	0	0.7
y	0.01	0	0.2
z	1	0.5	0.5

Table III. PD controller coefficients for the Tube MPC

controller	K_p	K_d
PD_1	-52.087	-22.98
PD_2	1	0
PD_3	1	0
PD_4	9.94	2.57

The results of applying two controllers to the system are Shown from Fig. 6 . to Fig. 7 . , This clearly shows the system's successful stabilization by the PID and Tube-MPC controller with position and Angles. Moreover, the system outputs have precisely attained the desired reference values. These visuals also illustrate the effective stabilization achieved by the Tube-MPC controller. To investigate the robustness of the design, a disturbance is added from second 5th onwards, which is the sum of a step function and a sinusoidal function with an amplitude of 0.7, to the values of ϕ, θ andψ.

The performance of PID and Tube-MPC controllers was evaluated for both position and angle response characteristics, using key control parameters: Rise Time (RT) and settling Time (ST) These parameters were extracted and analyzed based on the system's position (x,y,z) and angle (ϕ, θ, ψ) responses, specifically focusing on each controller's ability to achieve stability, precision, and rapid response.

The results of the position response for both PID and Tube-MPC controllers reveal a significant difference in their performance. Tube-MPC demonstrated a faster response across all axes, with lower rise times and settling times than PID. Furthermore, the Tube-MPC controller achieved zero overshoot for all position axes, indicating a more stable and precise control behavior. In contrast, the PID controller exhibited a noticeable overshoot, especially in the x and y axes, which could result in oscillations and prolonged settling times. This behavior illustrates the advantage of Tube-MPC in applications where quick and precise positioning is critical.

For the angle responses, the Tube-MPC controller also generally outperformed the PID controller in terms of rise time and settling time, especially in the ϕ and θ axes. The Tube-MPC reached the desired angle with minimal overshoot, ensuring smoother control. In the ψ axis, both controllers experienced high overshoot due to the inherent dynamics of this axis. Still, Tube-MPC achieved a faster settling time, indicating its ability to stabilize even in challenging conditions. This comparison demonstrates Tube-MPC's superiority in achieving quicker and more stable angular responses across multiple axes. All these changes have been calculated in Table IV and Table V, and for IAE and ISE in TableVI and Table VII.

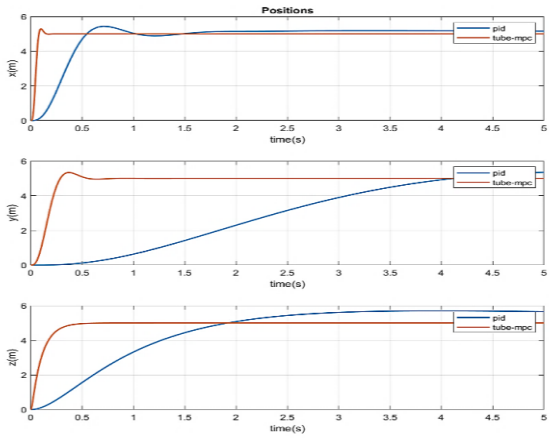


Fig. *6* . Comparison between PID and Tube-MPC position control

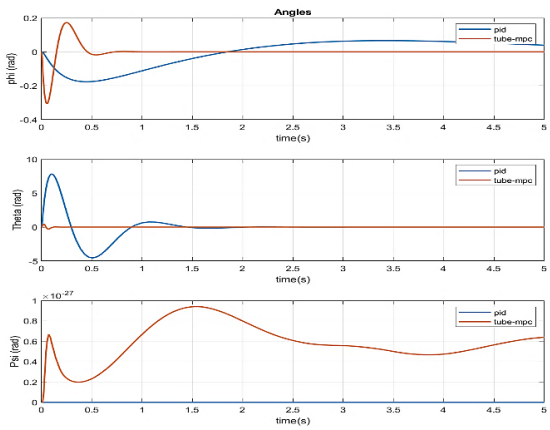


Fig. *7* . Comparison between PID and Tube-MPC attitude control

Table IV. COMPARISON OF CLASSICAL Angles PID AND Tube-MPC Controller

Angle	RT-pid	RT-Tube-mpc	OS-pid	OS-Tube-mpc	ST-pid	ST-Tube-mpc
Roll	0.3	0.15	0.15	0	1	0.5
Pitch	0.3	0.15	0.05	0.002	0.7	0.3
Yaw	0.4	0.3	0.4	0.3	2.5	2

Table V. COMPARISON OF CLASSICAL Position PID AND Tube-MPC Controller

Position	RT-pid	RT-Tube-mpc	OS-pid	OS-Tube-mpc	ST-pid	ST-Tube-mpc
x	0.3	0.15	1.2	0.01	1	0.6
y	1.2	0.3	0.4	0.3	5.1	0.6
z	1.5	0.2	0	0	3.5	0.5

Table VI. COMPARISON OF IAE and ISE for Angles PID AND Tube-MPC Controller

Angle	IAE-pid	IAE-Tube-mpc	ISE-pid	ISE-Tube-mpc
Roll	2.5	0.3	2	0.1
Pitch	1.8	0.2	1.5	0.1
Yaw	3.5	3	2	1.8

Table VII. COMPARISON OF IAE and ISE for Position PID AND Tube-MPC Controller

Position	IAE-pid	IAE-Tube-mpc	ISE-pid	ISE-Tube-mpc
x	3	1	2.5	0.5
y	5	1.2	4	0.6
z	4	0.8	3.5	0.4

B. Formation Control

The results reveal that the Tube-MPC controller effectively rejects disturbances and accurately controls all outputs. Ultimately, we explore a problem involving six agents and conduct comprehensive simulations to implement formation control on a nonlinear model.

At this juncture, it is essential to outline three scenarios to illustrate the controller's performance. The forthcoming discussion will encompass these scenarios, showcasing the robustness and precision of the Tube-MPC controller in various formation control task.

C. Formation Helix

In this scenario, we chose these parameters for the helix formation, adjoint matrix is shown in (35).

$$A = \begin{bmatrix} 0 & 1 & 1 & 1 & 1 & 1 \\ 1 & 0 & 1 & 1 & 1 & 1 \\ 1 & 1 & 0 & 1 & 1 & 1 \\ 1 & 1 & 1 & 0 & 1 & 1 \\ 1 & 1 & 1 & 1 & 0 & 1 \\ 1 & 1 & 1 & 1 & 1 & 0 \end{bmatrix} \tag{35}$$

Additionally, the desired distance matrix has been defined below:

$$d = \begin{bmatrix} 0 & 1.1756 & 1.9021 & 1.9021 & 1.1756 & 1 \\ 1.1756 & 0 & 1.1756 & 1.9021 & 1.9021 & 1 \\ 1.9021 & 1.1756 & 0 & 1.1756 & 1.9021 & 1 \\ 1.9021 & 1.9021 & 1.1756 & 0 & 1.1756 & 1 \\ 1.1756 & 1.9021 & 1.9021 & 1.1756 & 0 & 1 \\ 1 & 1 & 1 & 1 & 1 & 0 \end{bmatrix} \tag{36}$$

Furthermore, to achieve the formation among agents, The value of K_v has been set to 50, and K_1 has been set to 1 Q top from the helix formation for the three dimensions x, y, and z is established in Equation (37)

$$\begin{aligned} x_r &= 5\,sin\frac{\pi}{20}t \\ y_r &= 5\,cos\frac{\pi}{20}t \\ z_r &= 0.1t \end{aligned} \tag{37}$$

The value of the target velocity, assumed to be estimated, is represented below:

$$\hat{v}_T = \begin{bmatrix} \frac{\pi}{4}cos\frac{\pi}{20}t \\ -\frac{\pi}{4}sin\frac{\pi}{20}t \\ 0.1 \end{bmatrix} \tag{38}$$

Therefore, the chart of the formation factors is illustrated in Fig. 8 . Based on Fig. 8 . , it can be concluded that all six

controlled nonlinear dynamic factors have successfully reached the desired formation and can follow the helix formation. Therefore, the results indicate that controlled system dynamics can be employed instead of conventional formation methods to format agents . This involves initially controlling the agents using an internal controller and then applying the specified formulas to the system dynamics, determining the path for helix formation so that they reach a defined form and can be accurately tracked.

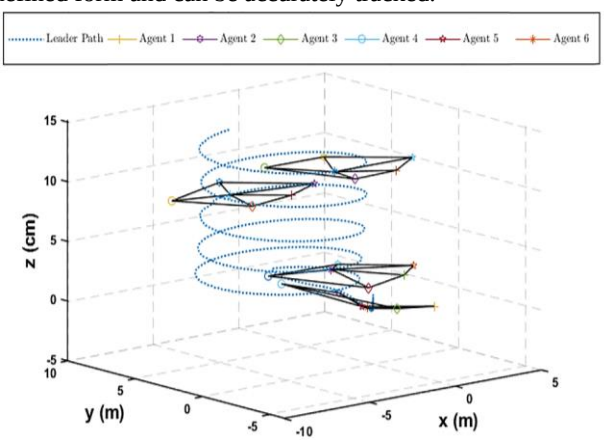


Fig. *8* . Agents' formation in desired path

a) Formation and Obstacle Avoidance

Now, 6 agents choose a line formation and track a particular path. An obstacle is positioned in the path's middle, and agents must bypass it within a determined distance. Parameters of obstacle-avoiding formation are depicted in Table VIII. And it's present in Fig. 9 .

Table VIII. obstacle avoiding formation parameters

symbol	*parameter*	*value*
r_a	*Obstacle radios*	5
k_r	*Constant coefficient*	0.05
k_a	*Constant coefficient*	10
K	*Constant coefficient*	10
q_0	*Circle position*	(10,10,2.5)

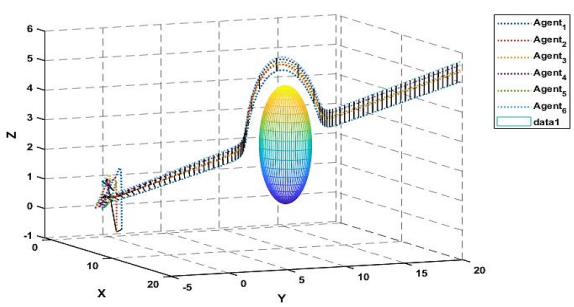


Fig. *9* . Obstacle avoiding formation

D. Variation formation

In this section, time-varying formation is considered. Before the 50s, formation was as a line, and afterward, it was changed to a pentagon shape, as illustrated in Fig. 10 . The Z trajectory is considered zero in the plotting. It is evident from Fig. 10 that agents have to keep their line formation while avoiding the collision through the trajectory. Parameters and gains regarding this formation are shown in Table IX. For better illustration, time-varying formation in 2D can be seen in Fig. 11 .

TABLE IX. VARIATION FORMATION PARAMETERS

symbol	*parameter*	*value*
λ_1	*Constant coefficient*	5
λ_2	*Constant coefficient*	5
t_s	*Formation transition time*	50
τ	*Exponential rate*	10
d_1^1	*Desired distance*	$[0 \quad 6]^T$
d_1^2	*Desired distance*	$[0 \quad 2]^T$
d_2^1	*Desired distance*	$[0 \quad 4]^T$
d_2^2	*Desired distance*	$[2\cos(18) \quad 2\,sin(18)]^T$
d_3^1	*Desired distance*	$[0 \quad 2]^T$
d_3^2	*Desired distance*	$[-2\cos(18) \quad 2\,sin(18)]^T$
d_4^1	*Desired distance*	$[0 \quad -2]^T$
d_4^2	*Desired distance*	$[2\cos(54) \quad -2sin(54)]^T$
d_5^1	*Desired distance*	$[0 \quad -4]^T$
d_5^2	*Desired distance*	$[-2\cos(54) \quad -2sin(54)]^T$

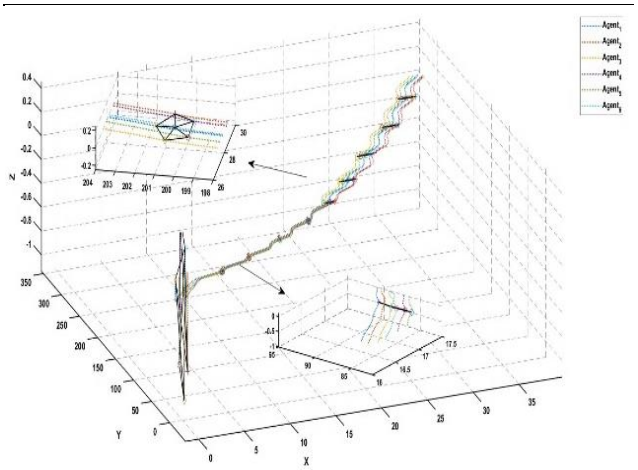


Fig. *10* . pentagonal formation in variation formation

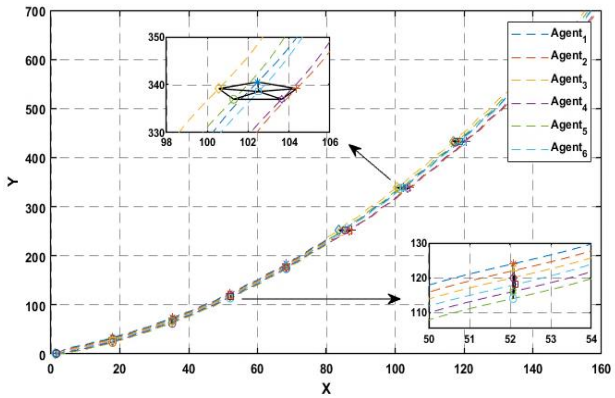


Fig. *11* . variation formation

VI. Conclusion

In this paper, after investigating the nonlinear model of a quadcopter as a case study and examining its parameters, the analysis of the linearized quadcopter system was undertaken and introduced its state space model. In the first section, the control objective is to pursue position control in the nonlinear quadcopter system using a PID controller. For this purpose, six PID controllers were utilized and coefficients were determined to control all system outputs effectively. By examining the system output plots, it is observed that the assigned coefficients appropriately regulate the outputs. A constrained Tube-MPC controller was designed for the nonlinear system in the following section. By examining the plots of the Tube-MPC controller and comparing it with the PID controller, it was concluded that Tube-MPC controlled the outputs better than the PID controller when constraints were considered. Also, according to the physical limitations of the quadcopter, the Tube-MPC controller can apply better control inputs to the system than the PID controller. In the following section, the article's objective was to design a formation for a group of six quadcopters considering nonlinear dynamics, such that, in addition to achieving a specific formation. We first reviewed the formation theories to accomplish this goal and then attempted to implement them on the controlled nonlinear dynamics using a nonlinear PID controller. Simulating this problem and examining the plots, the implemented method successfully utilizes the controlled nonlinear system dynamics to reach an appropriate form.

References

[1] D. Yan, W. Zhang, and H. Chen, "Design of a multi-constraint formation controller based on improved MPC and consensus for quadrotors," *Aerospace*, vol. 9, no. 2, p. 94, 2022.

[2] S. Y. Ku, G. Nejat, and B. Benhabib, "Wilderness search for lost persons using a multimodal aerial-terrestrial robot team," Robotics, vol. 11, no. 3, p. 64, 2022.

[3] M. Sharma, A. Gupta, S. K. Gupta, S. H. Alsamhi, and A. V. Shvetsov, "Survey on unmanned aerial vehicle for Mars exploration: Deployment use case," Drones, vol. 6, no. 1, p. 4, 2022.

[4] Q. Zong, D. Wang, S. Shao, B. Zhang, and Y. Han, "Research status and development of multi UAV coordinated formation flight control," Journal of Harbin Institute of Technology, vol. 49, no. 3, pp. 1-14, 2017.

[5] X. Fu, J. Pan, H. Wang, and X. Gao, "A formation maintenance and reconstruction method of UAV swarm based on distributed control," Aerospace Science and Technology, vol. 104, p. 105981, 2020.

[6] G. Hoffmann, H. Huang, S. Waslander, and C. Tomlin, "Quadrotor helicopter flight dynamics and control: Theory and experiment," in AIAA guidance, navigation and control conference and exhibit, 2007, p. 6461.

[7] H. Huang, G. M. Hoffmann, S. L. Waslander, and C. J. Tomlin, "Aerodynamics and control of autonomous quadrotor helicopters in aggressive maneuvering," in 2009 IEEE international conference on robotics and automation, 2009: IEEE, pp. 3277-3282.

[8] C. E. Garcia, D. M. Prett, and M. Morari, "Model predictive control: Theory and practice—A survey," Automatica, vol. 25, no. 3, pp. 335-348, 1989.

[9] F. Allgöwer and A. Zheng, Nonlinear model predictive control. Birkhäuser, 2012.

[10] S. Wolfe, S. Givigi, and C.-A. Rabbath, "Distributed multiple model mpc for target tracking uavs," in 2020 International Conference on Unmanned Aircraft Systems (ICUAS), 2020: IEEE, pp. 123-130.

[11] Y. Kuriki and T. Namerikawa, "Formation control with collision avoidance for a multi-UAV system using decentralized MPC and consensus-based control," SICE Journal of Control, Measurement, and System Integration, vol. 8, no. 4, pp. 285-294, 2015.

[12] H.-T. Do and I. Prodan, "Experimental validation of an explicit flatness-based MPC design for quadcopter position tracking," arXiv preprint arXiv:2308.15946, 2023.

[13] Z. Chao, S.-L. Zhou, L. Ming, and W.-G. Zhang, "UAV formation flight based on nonlinear model predictive control," Mathematical Problems in Engineering, vol. 2012, no. 1, p. 261367, 2012.

[14] A. Bemporad and M. Morari, "Robust model predictive control: A survey," in Robustness in identification and control: Springer, 2007, pp. 207-226.

[15] Y. Wang and S. Boyd, "Fast model predictive control using online optimization," IEEE Transactions on control systems technology, vol. 18, no. 2, pp. 267-278, 2009.

[16] A. Richards and J. How, "Implementation of robust decentralized model predictive control," in AIAA Guidance, Navigation, and Control Conference and Exhibit, 2005, p. 6366.

[17] T. Schouwenaars, J. How, and E. Feron, "Decentralized cooperative trajectory planning of multiple aircraft with hard safety guarantees," in AIAA Guidance, Navigation, and Control Conference and Exhibit, 2004, p. 5141.

[18] G. V. Raffo, M. G. Ortega, and F. R. Rubio, "An integral predictive/nonlinear H∞ control structure for a quadrotor helicopter," Automatica, vol. 46, no. 1, pp. 29-39, 2010.

[19] Z. Zuo, "Trajectory tracking control design with command-filtered compensation for a quadrotor," IET control theory & applications, vol. 4, no. 11, pp. 2343-2355, 2010.

[20] S. Bouabdallah, A. Noth, and R. Siegwart, "PID vs LQ control techniques applied to an indoor micro quadrotor," in 2004 IEEE/RSJ International Conference on Intelligent Robots and Systems (IROS)(IEEE Cat. No. 04CH37566), 2004, vol. 3: IEEE, pp. 2451-2456.

[21] K. Alexis, G. Nikolakopoulos, and A. Tzes, "Experimental

constrained optimal attitude control of a quadrotor subject to wind disturbances," International Journal of Control, Automation and Systems, vol. 12, pp. 1289-1302, 2014.
[22] X. Yang, H. Pota, and M. Garratt, "Design of a gust-attenuation controller for landing operations of unmanned autonomous helicopters," in 2009 IEEE Control Applications,(CCA) & Intelligent Control,(ISIC), 2009: IEEE, pp. 1300-1305.
[23] T. Luukkonen, "Modelling and control of quadcopter," Independent research project in applied mathematics, Espoo, vol. 22, no. 22, 2011.
[24] S. Norouzi Ghazbi, A. A. Akbari, and M. Gharib, "Quadrotor Full dynamic Modeling, Nonlinear Simulation and Control of Attitudes," Indian Journal of Scientific Research, vol. 1, 2014.
[25] S. Ariram, J. Röning, and Z. Kowalczuk, "Implementation of control system and tracking objects in a quadcopter system," in Interactive Collaborative Robotics: 4th International Conference, ICR 2019, Istanbul, Turkey, August 20–25, 2019, Proceedings 4, 2019: Springer, pp. 19-29.
[26] S. Abdelhay and A. Zakriti, "Modeling of a quadcopter trajectory tracking system using PID controller," Procedia Manufacturing, vol. 32, pp. 564-571, 2019.
[27] S. Vargas, H. M. Becerra, and J.-B. Hayet, "MPC-based distributed formation control of multiple quadcopters with obstacle avoidance and connectivity maintenance," Control Engineering Practice, vol. 121, p. 105054, 2022.
[28] D. F. S. De Sá and J. V. D. F. Neto, "Multi-Agent Collision Avoidance System Based on Centralization and Decentralization Control for UAV Applications," IEEE Access, vol. 11, pp. 7031-7042, 2023.
[29] M. De Queiroz, X. Cai, and M. Feemster, Formation control of multi-agent systems: a graph rigidity approach. John Wiley & Sons, 2019.
[30] H.-T. Do and I. Prodan, "Tube MPC via flatness for multicopter trajectory tracking," in 2024 European Control Conference (ECC), 2024: IEEE, pp. 1449-1454.
[31] H. A. Hassan, "Tube-based NMPC for Non-Holonomic," rn (xk, uk), vol. 2, p. 47, 2024.
[32] S.-S. Liu, T.-F. Ding, M.-F. Ge, X.-G. Dong, and Z.-W. Liu, "Multiquadrotor Formation Tracking with Mixed Constraints: A Hierarchical Rolling Optimization Approach," IEEE Transactions on Aerospace and Electronic Systems, vol. 59, no. 5, pp. 7269-7280, 2023.
[33] F. Borrelli, A. Bemporad, and M. Morari, Predictive control for linear and hybrid systems. Cambridge University Press, 2017.
[34] L. F. C. Ccari and P. R. Yanyachi, "A Novel Neural Network-Based Robust Adaptive Formation Control for Cooperative Transport of a Payload Using Two Underactuated Quadcopters," IEEE Access, vol. 11, pp. 36015-36028, 2023.
[35] D. Shen and Q. Lu, "Hierarchical formation control with applications to multi-quadrotor systems," IEEE Access, vol. 7, pp. 130599-130609, 2019.
[36] A. Azarbahram, N. Pariz, M. B. Naghibi-Sistani, and R. Kardehi Moghaddam, "Leader-Follower Formation Control of Uncertain USV Networks Under Stochastic Disturbances," International Journal of Industrial Electronics Control and Optimization, vol. 5, no. 2, pp. 133-142, 2022.
[37] S. Khankalantary, I. Izadi, and F. Sheikholeslam, "Robust ADP-based solution of a class of nonlinear multi-agent systems with input saturation and collision avoidance constraints," ISA transactions, vol. 107, pp. 52-62, 2020.
[38] N. H. Sahrir and M. A. Mohd Basri, "Modelling and manual tuning PID control of quadcopter," in Control, instrumentation and mechatronics: Theory and practice: Springer, 2022, pp. 346-357.
[39] S. D. Sahputro, F. Fadilah, N. A. Wicaksono, and F. Yusivar, "Design and implementation of adaptive PID controller for speed control of DC motor," in 2017 15th International Conference on Quality in Research (QiR): International Symposium on Electrical and Computer Engineering, 2017: IEEE, pp. 179-183.
[40] J.-W. Lee, N. Xuan-Mung, N. P. Nguyen, and S. K. Hong, "Adaptive altitude flight control of quadcopter under ground effect and time-varying load: Theory and experiments," Journal of Vibration and Control, vol. 29, no. 3-4, pp. 571-581, 2023.
[41] N. Xuan Mung, N. P. Nguyen, D. B. Pham, N. N. Dao, and S. K. Hong, "Synthesized landing strategy for quadcopter to land precisely on a vertically moving apron," Mathematics, vol. 10, no. 8, p. 1328, 2022.



Seyedeh Mahsa Zakipour Bahambari was born in 1999. She received her B.S. degree in Electrical Engineering in 2022. She is currently an M.Sc. student in Mechatronics Engineering at K. N. Toosi University of Technology under supervision of Assistant Professor Saeed Khankalantary. She has found her field of interest in multi-agent systems, specifically in the formation of Quadcopters. She has an extensive experience in programming languages, including MATLAB, C++, Phyton, and Simulink.



Saeed Khankalantary was born in 1991. He received his B.S. degree in Electrical Engineering in 2012 from Yazd University, Yazd, Iran, and M.S. degree in Control Engineering in 2014 from K. N. Toosi University of Technology, Tehran, Iran. He wrote his dissertation under the supervision of Prof. Mohammad Teshnelab. He received his PhD degree at the Isfahan University of Technology, Isfahan, Iran, in 2020. He is currently an Assistant Professor at the Department of Mechatronics, Faculty of Electrical Engineering, K. N. Toosi University of Technology. His research interests are Multi-agent Control Systems, Estimation Theory, Intelligent Control, Sensor Fusion, and Mechatronics.

.